Appl Phys B (2008) 93: 521–529
DOI 10.1007/s00340-008-3211-3

Applied Physics B
Lasers and Optics

Dynamics of two coupled erbium-doped fiber ring lasers in transient regime

J.A. Sánchez-Martín · J. Used · J.C. Martín

Received: 1 April 2008 / Revised version: 3 July 2008 / Published online: 20 September 2008

Abstract The transient of an erbium-doped fiber ring laser coupled to another one receiving CW pump power is studied. The transient signals experimentally obtained may present different profiles depending on several conditions (degree of coupling between both lasers, pump powers of each one, etc.). In particular, an appropriate choice of working conditions makes possible to suppress relaxation oscillations and to shorten the time elapsed since the moment of pump switch-on till steady state. A model is proposed in which inclusion of polarization hole burning has been necessary to achieve an acceptable agreement with the transient behaviors experimentally observed.

PACS 42.55.Wd · 42.60.Rn

1 Introduction

Relaxation oscillations constitute a well known phenomenon observed in the transient of class B lasers after pump switch on. It was already reported in the very first ruby lasers [1] and it has been analyzed for a wide variety of purposes, either purely basic [2–5], aimed to the active medium characterization [6–9], or focused on features detailed next. Dynamics of class B lasers with coupled multimode emission exhibit antiphase behavior, regardless of whether the coupling is due to cross saturation [2, 10–12] or other mechanisms such as intracavity second-harmonic generation [13, 14]. Antiphase dynamics is interesting for nonlinear dynamics science due to its complexity and for laser science due to the mechanisms that it reveals: for instance, in an EDF laser, its transient can be modeled by treating the active medium as homogeneous [8, 9] if one only deals with the total laser power. Nevertheless, antiphase behavior in the relaxation oscillations of polarization modes is explained by means of the polarization hole-burning (PHB) effect, which makes it clear the inhomogeneous behavior of the active medium.

On the other hand, different authors have studied methods for smoothing the relaxation oscillations. In applications with a laser power breakout limit, the CW laser level must be much lower than the safety limit in order that the first transient peaks do not exceed it, as their power is considerably greater than the one corresponding to the steady state. Nevertheless, if the transient peaks are minimized, CW power can be safely increased. In order to achieve this, several methods have been proposed. Some of them are based on increasing the cavity loss for high laser emission, either by including nonlinear elements within the resonator so that their losses grow with the laser power, or by external feedback systems which cause a similar effect [15–17]. Some other procedures proposed are the laser steering or steady state targeting techniques [18–20], which basically consist of tailoring the pump power temporal profile: instead of simply switching-on the pump source, which would amount to using a step pump temporal profile, other profiles are employed. Finally, in optical fiber lasers, smoothing of the laser power temporal profile by means of a phase shift between the temporal responses of each polarization mode has been demonstrated [21].

The system analyzed in this work consists of two coupled EDF ring lasers. In particular, we have studied the transient taking place after pump switch-on of one laser (called

J.A. Sánchez-Martín · J. Used · J.C. Martín (✉)
Departamento de Física Aplicada, Instituto de Investigación en Ingeniería de Aragón (I3A), Universidad de Zaragoza, C/Pedro Cerbuna, 12, 50009 Zaragoza, Spain
e-mail: jcmartin@unizar.es
Fax: +34-976-761233

here the "main" one), if previously the other laser (called the "secondary" one) had been switched on and had reached the steady state. This process is more complex than the conventional transient in class B lasers because in this case each laser possesses two polarization modes, coupled via the active medium that they share, and both lasers are coupled as well. As the power present in each laser is not entirely generated by itself, its transient does not follow the typical relaxation oscillations pattern. Instead, a variety of patters can be observed, depending on the degree of coupling between both cavities. In particular, if the pump powers launched to the lasers and the degree of coupling are conveniently selected, oscillations after pump switch on can be eliminated, so that the transient consists of a monotonous laser power increase. Besides, it is possible to get the steady state faster than in a single laser, which might be a feature of interest for commutation applications.

The phenomena observed are qualitatively reproduced by a model proposed by us, which is based on previous models of erbium-doped fiber laser dynamics, some of them including the PHB effect [3, 10, 22]. The acceptable numerical results obtained point out that the model proposed contains all the significant ingredients necessary to explain the phenomena experimentally observed.

2 Experimental setup and results

Figure 1 shows the experimental setup. Both rings contain similar (but not identical) components, although they are arranged in different order in each ring: a multiplexer (1480/1550 nm) with which pump power is coupled, a length of erbium-doped fiber (12 m in the main ring and 27 m in the secondary one), a tunable filter which must be tuned almost to the same wavelength in both rings (later we discuss this point more precisely), an isolator which allows laser signal propagation in the opposite sense to the pump propagation one, and a coupler as laser signal output (not necessary in the secondary laser in order to smooth the transient of the main one, but useful to carry out the study). Besides, both rings share a variable coupler that makes possible the exchange of part of the laser signal between both cavities.

Further on, we will refer to the ring at the left hand side of Fig. 1 as the main ring, or ring a, and we focus our study on this ring's output. The other ring will be called the secondary ring, or ring b. For both rings, the wavelength of the pump employed is 1480 nm. The secondary ring is fed by a CW pump power $P_{p,b}$, while the main ring receives a square-wave modulated pump power ($P_{p,a}$) so that the pump is completely interrupted in the low phase of the square-wave. Output ports are connected to PIN photodiodes whose voltage signals are registered by a digital oscilloscope triggered by the function generator used to modulate the pump power of the main ring.

Figure 2 shows the temporal evolution of the main ring output after $P_{p,a}$ switch-on (instant chosen as time origin), for different coupling ratios. All the $P_{p,a}$ and $P_{p,b}$ values provided in this article refer to the magnitudes at the active fiber input end. This feature is expressed by the parameter w,

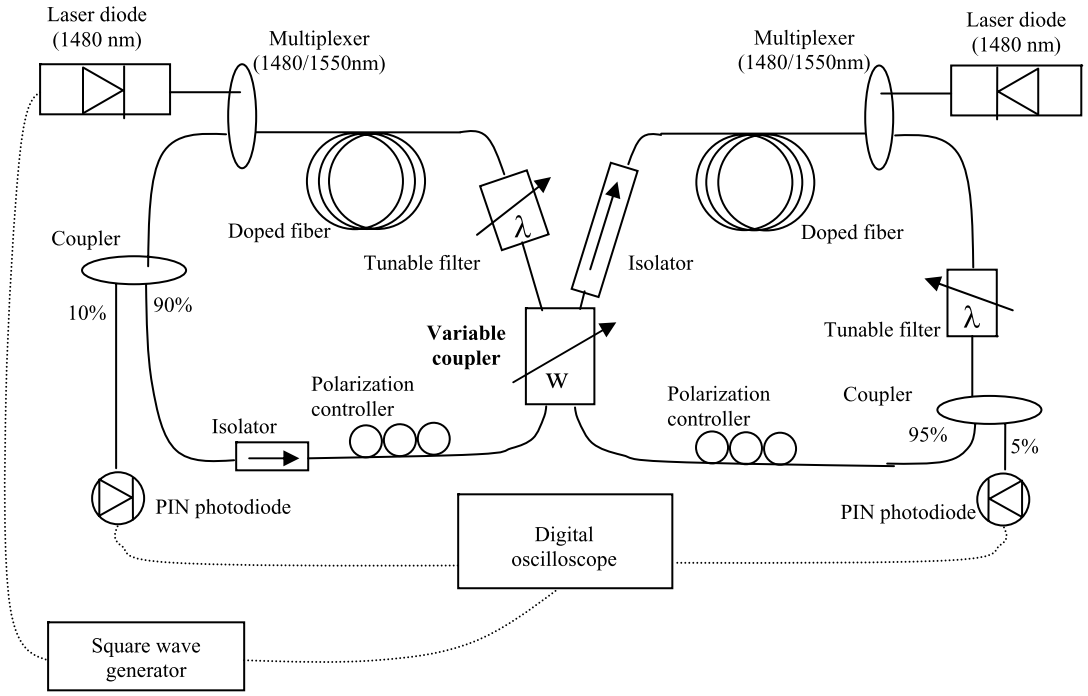

Fig. 1 Experimental setup, with the main ring at the *left hand side* and the secondary ring at the *right hand side*

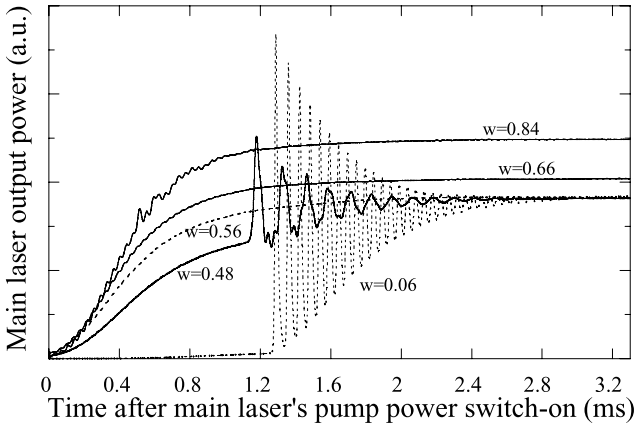

Fig. 2 Temporal evolution of the main ring output laser emission after switch-on of its pump power, for several w values. $P_{p,a} = 41$ mW; $P_{p,b} = 36$ mW

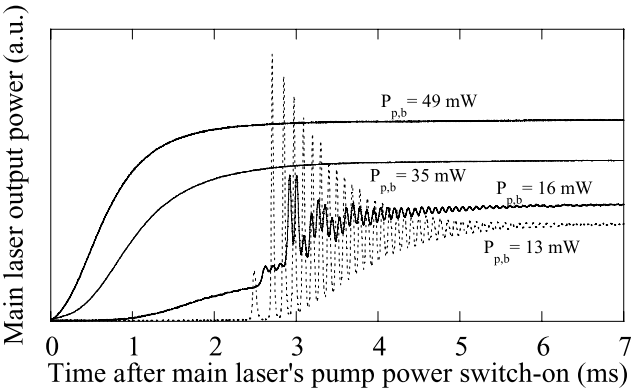

Fig. 4 Temporal evolution of the main ring output laser emission after switch-on of its pump power, for several $P_{p,b}$ values. $P_{p,a} = 40$ mW; $w = 0.30$

Fig. 3 Scheme for the definition of the w parameter

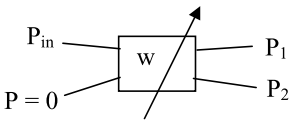

defined according to Fig. 3 and the expression:

$$w = \frac{P_2}{P_1 + P_2} \tag{1}$$

(obviously, the variable coupler is not an ideal device, that is to say, $P_1 + P_2 < P_{\text{in}}$). The curve corresponding to $w = 0.06$ represents a situation in which the main ring works almost on its own, without the influence of the secondary. It can be observed how the transient first peak exhibits a power around twice the one corresponding to the steady state. As long as the coupling factor increases, oscillations become more irregular (see representative curve for $w = 0.48$). If the coupling factor is still increased, oscillations observed are negligible. Besides, the laser power in the main ring becomes enforced with regard to its value with $w = 0.06$. Therefore, in this working condition the secondary ring not only prevents the appearance of high power peaks, but it also contributes to raise the output power of the device.

It is also remarkable that the time elapsed since $t = 0$ until establishment of the steady state can also be reduced with the appropriate w: for $w = 0.56$ or greater, it can be estimated that the steady state is reached 1.5 ms after pump power switch on, while for $w = 0.06$ the steady state is not reached until 3 ms after pump power switch on.

In Fig. 4, the transient profile dependence on the secondary ring pump power ($P_{p,b}$) can be appreciated: for low values of $P_{p,b}$, the transient profile observed matches the relaxation oscillations typical scheme save for the appearance of one emission peak (in other conditions, two or three) before the greatest emission peak; for a certain range of $P_{p,b}$, the transient profile becomes more complex (case corresponding to $P_{p,b} = 16$ mW is representative); finally, if $P_{p,b}$ is high enough, a smooth transient is obtained (as is logical, the larger the $P_{p,b}$ value, the more the steady state level).

Note that the main laser output power (P_{lout}) is negligible at $t = 0$. This feature of the system is favored by the arrangement of the secondary ring components, by the moderate pump power launched to it and by the wavelength selected, corresponding to maximum absorption. These conditions can be modified if there is no need for a complete interruption of the main laser emission before $P_{p,a}$ switch-on: $P_{p,b}$ can be raised, so that a greater P_{lout} can be achieved and the steady state can be reached faster. On the other hand, efficiency can be increased by modifying the arrangement of the secondary ring's components (apart from suppressing the output coupler). Observe that in the secondary ring in Fig. 1, P_{lout} maximum is reached at the doped fiber end by which light exits the active medium, but before this light arrives at the variable coupler it passes through the tunable filter, whose transmission losses are 3.2 dB. This filter can be moved, for instance, to be placed between the isolator and the doped fiber. With such a configuration, the steady state output power of the main ring is strongly increased and the transient duration is reduced, but in these conditions $P_{p,a}$ switch-off does not lead to complete interruption of P_{lout}.

It is convenient to clear up that the experimental study summarized by the different series presented here spread over different days, which is far longer than the time that a polarization-depending fiber system can be kept stable. This fact explains the apparent discrepancy between Fig. 2 and the transient of Fig. 4 corresponding to $P_{p,b} = 35$ mW: the pump power conditions of the latter being practically the same than the ones in Fig. 2 and the w value being 0.30, relaxation oscillations should appear according to the trend shown in Fig. 2. Nevertheless, the mentioned transient in Fig. 4 is totally smoothed. This fact can be understood taking into account that series corresponding to Figs. 2 and 4

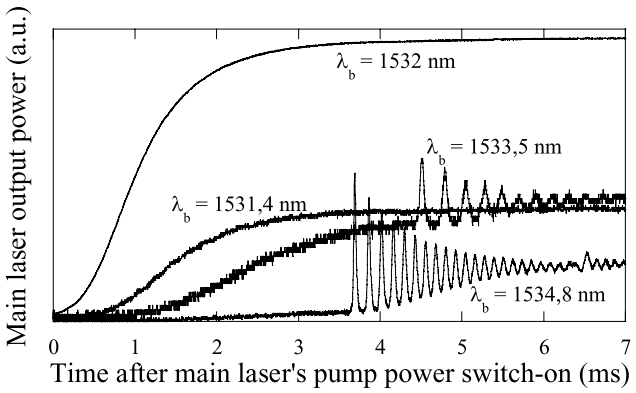

Fig. 5 Temporal evolution of the main ring output laser emission ($\lambda_a = 1532.2$ nm) after switch-on of its pump power, for different tuned wavelengths in the secondary ring. $P_{p,a} = 40$ mW; $P_{p,b} = 35$ mW; $w = 0.30$

were not measured consecutively, so it is not surprising that the state of the system changed between the recordings of both series.

Figure 5 illustrates the changes in the main ring laser transient as a function of the tuning wavelength mismatch between both rings. If the wavelength mismatch exceeds the filter bandwidth ($\lambda_b = 1534.8$ nm), influence between both rings is very low. In these conditions, the system is very inefficient and the transient obtained follows the typical relaxation oscillations scheme. As long as the wavelength mismatch is reduced, the system efficiency increases and the relaxation oscillations diminish and even disappear. Nevertheless, if the tuned wavelengths of both rings are very close, the emission becomes unstable as the oscillators approach the phase locking condition [23, 24]. A spectral analysis by means of a Brillouin Optical Spectrum Analyzer [25] reveals a change of regime depending on the tuning wavelength mismatch: if it is high enough, only one or two lines are observed (Fig. 6(a)) whose wavelengths and powers slightly fluctuate while, if the mismatch is low enough, many more lines appear (Fig. 6(b)). Therefore, in order to achieve a stable and efficient performance of the system, the ring tuning wavelengths must be slightly mismatched. On the other hand, this property might be interesting for accurate tuning of one laser to another laser's wavelength used as a reference: if both can be coupled (as it is the case of erbium-doped fiber lasers), whether the tune is right can be detected by observing whether the laser signal is unstable.

Finally, it must be pointed out that the transient profiles can be significantly modified by means of the polarization controllers. The most representative profiles have been shown in the preceding figures, but also some more exotic transients can be found, such as the ones illustrated in Fig. 7.

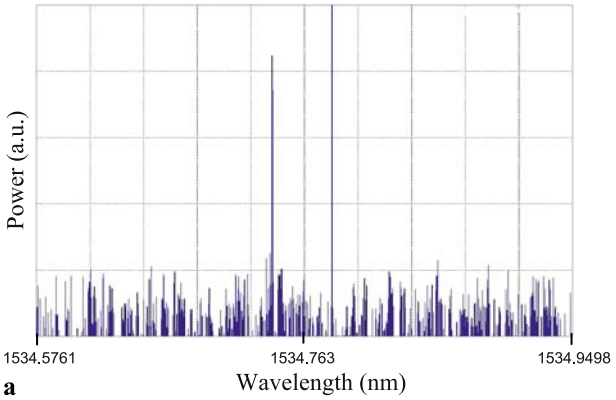

Fig. 6 Main ring output signal spectrum for two different tuning wavelength mismatches (greater in (**a**) than in (**b**))

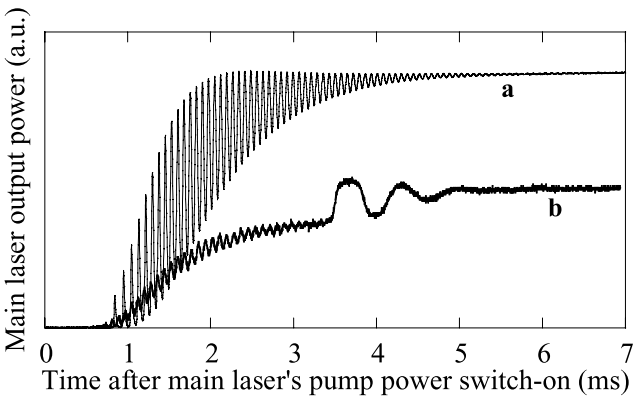

Fig. 7 Temporal evolution of the main ring output laser emission after switch-on of its pump power, for $w = 0.66$ (**a**) and for $w = 0.56$ (**b**). $P_{p,a} = 39$ mW; $P_{p,b} = 13$ mW

3 Theoretical model

In the system under study, different interrelated phenomena take place. In order to elucidate which ones are fundamental to explain the effects observed, the procedure followed consisted of comparing the experimental results with the ones generated by different models, starting from a simple ver-

sion which was subsequently completed by including new effects, until an acceptable agreement between experimental and theoretical results was achieved. According to this approach, the starting point to model the system was based on the EDFL ring model explained in [22], in which the active medium is treated as homogeneous and the laser radiation is treated as single-mode. For a single laser (not coupled), this model suffices to explain the dynamics observed, as it provides the typical relaxation oscillations. Nevertheless, when considering homogeneous treatment for two coupled lasers the results were not satisfactory, as the only transient profiles obtained reduced to the relaxation oscillations scheme, but none of the other behaviors shown in the preceding figures (smooth transient or irregular oscillations) appeared.

The next step was considering PHB. This phenomenon is due to several factors: on the one hand, the random nature of the glass host makes each Er^{3+} ion have a different sensitivity to polarization. On the other hand, pump light is polarized so that the probability of population inversion is host dependent. Therefore, the gain provided by the active medium is also polarization dependent. The two cavity polarization eigenmodes present different gains and, besides, they are mutually dependent as both eigenmodes share the same active medium. The simplest models including PHB for the treatment of rare-earth doped fibers resource to average quantities such as two assemblies of active ions, each one interacting directly to one polarization mode and through a coupling factor to the other polarization mode [3, 10] or three assemblies of active ions, two of them interacting exclusively with one polarization mode and the third one interacting with both modes [2, 12]. We choose the one based on two assemblies of active ions because it is slightly simpler than the model based on three assemblies. We assume as usual a two level scheme for the treatment of EDF lasers, so that in our model for a double ring configuration, we deal with four normalized upper level populations of each assembly (N_{ax}, N_{ay}, N_{bx} and N_{by}) and four laser modes with spatially averaged powers P_{ax}, P_{ay}, P_{bx}, and P_{by}. The first subscript refers to the ring (a for the main one, b for the secondary one) and the second subscript (x or y) labels each polarization eigenmode.

Further on, we will use the following subscripts notation for the sake of generality: $i = a$ or b and $j = b$ or a (always $i \neq j$), while $u = x$ or y and $v = y$ or x (always $u \neq v$). Interaction of the assembly u with the polarization eigenmode u is considered proportional to P_{iu}, while interaction of the assembly u with the polarization eigenmode v is considered proportional to $\beta_i P_{iv}$, where β_i is a coupling factor ($0 \leq \beta_i \leq 1$) similar to the one introduced in [2, 10, 11]. This way, the temporal evolution of N_{iu} is given by:

$$\dot{N}_{iu} = S_{1iu} - S_{2iu} N_{iu} + S_3(P_{iu} + \beta P_{iv}) - S_4(P_{iu} + \beta P_{iv}) N_{iu}. \quad (2)$$

The S coefficients are adaptations of the ones given in [22]:

$$S_{1iu} = \frac{\gamma_a(\nu_p)}{h\nu_p N_t} P_{pi}\delta_{iu}, \quad (3)$$

$$S_{2iu} = \frac{(\gamma_a(\nu_p) + \gamma_e(\nu_p))}{h\nu_p N_t} P_{pi}\delta_{iu} + \frac{1}{\tau}, \quad (4)$$

$$S_3 = \frac{\gamma_a(\nu_l)}{h\nu_l N_t}, \quad (5)$$

$$S_4 = \frac{(\gamma_a(\nu_l) + \gamma_e(\nu_l))}{h\nu_l N_t}. \quad (6)$$

In the preceding expressions, h is the Planck constant, N_t is half the number of Er^{3+} ions per unit length, that is to say, the number of Er^{3+} ions per unit length per assembly, ν_p and ν_l are the pump and laser signal optical frequencies, γ_a and γ_e represent the absorption and emission coefficients, and τ is the laser transition lifetime. For the sake of simplicity, it is assumed that the same kind of EDF is employed in both rings, as it happens in our experimental setup (of course, if the EDFs of both rings are not the same, different τ, γ_a, γ_e, and N_t must be used for each cavity). The pump launched to each ring is polarized so that both erbium assemblies are not necessarily affected the same way. We suppose that the polarization eigenmodes X and Y of ring i receive, respectively, ratios δ_{ix} and δ_{iy} of the total pump power ($\delta_{ix} + \delta_{iy} = 1$). Concerning the powers appearing in (2), they are average magnitudes along the EDF: as proved in [9], for EDF transient treatment it is a good approximation to introduce in the model:

$$P_{iu} = \frac{P_{iu}^{\text{in}} + P_{iu}^{\text{out}}}{2} \quad (7)$$

(P_{iu}^{in} and P_{iu}^{out} represent the powers of mode u at the laser signal input and output ends of the active fiber of ring i).

Let us analyze the coupling between both rings. Power that one ring receives from the other is projected on the eigenmodes of the first one. We call α the u mode power of ring i transmitted to the u mode power of ring j divided by the total u mode power of ring i. Obviously, mode v of ring j receives a ratio $1-\alpha$ out of the whole u mode power transmitted from ring i to ring j. Each eigenmode power evolves along the ring affected by passive components before and after the doped fiber, with respective global transmission factors $T_{i,\text{in}}$ and $T_{i,\text{out}}$ (Fig. 8), by the gain provided by the EDF and by the power exchange in the variable coupler. So, as an example, the powers transmitted from the mode X at the doped fiber output end of ring a to the modes X and Y at the doped fiber input end of ring b are $T_{a,\text{out}} w T_{b,\text{in}} \alpha P_{ax}^{\text{out}}$ and $T_{a,\text{out}} w T_{b,\text{in}} (1-\alpha) P_{ax}^{\text{out}}$, respectively (passive losses due to the variable coupler are included in the $T_{i,\text{out}}$ coefficients).

In the former section we pointed out that, in order to obtain a stable laser output, a mismatch in wavelength tuning

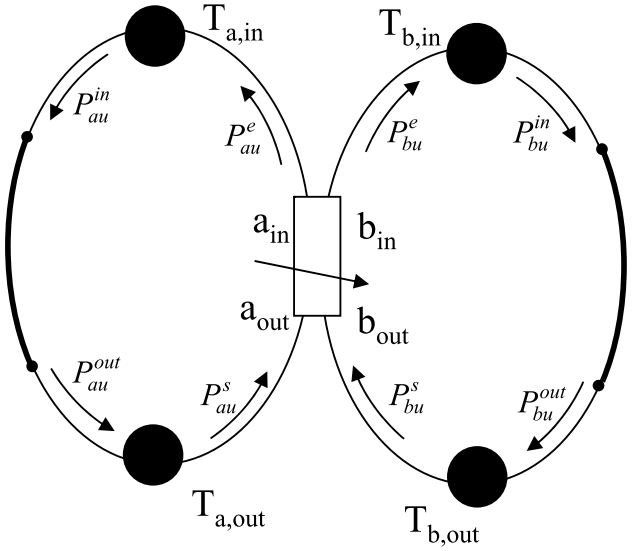

Fig. 8 Double ring simplified scheme. *Black circles* represent sets of passive components. The *thick solid line* represents the active fiber

between both rings was necessary. If the tuned wavelengths in rings a and b are λ_a and λ_b, it is clear that, when there is coupling between the rings and both are pumped above threshold, we can consider that the spectrum of the radiation present in both of them reduces to these two wavelengths (we neglect chirp effects). We consider that the laser powers P_{iu} in (2) are the sum of two contributions whose wavelengths are λ_i and λ_j: $P_{iu} = P_{iiu} + P_{iju}$. The second subscript points out the corresponding wavelength. The temporal evolution of P_{iiu} can be formulated by adapting expressions proposed for a single cavity [8, 22] to our system of two coupled cavities:

$$P_{iiu}(t+\Delta t) = P_{iiu}(t)\{T_{i,\text{in}} G_{iu} T_{i,\text{out}} F_{iu}\}^{\frac{c\Delta t}{D_i}}, \tag{8}$$

where D_i is the optical path of ring i, Δt is the time step employed for the numerical calculation, G_{iu} is the gain provided to mode u by the doped fiber in ring i and F_{iu} is the ratio P^e_{iiu}/P^s_{iiu}, where the meaning of the subscripts "e" and "s" are defined by means of Fig. 8. Concerning the gain provided by the active medium to mode u, it must be taken into account that the assembly v also contributes: this way, the emission coefficient for the propagation of mode u is $\gamma_e(\nu_l)(N_{iu} + \beta N_{iv})$, while the absorption coefficient is $\gamma_a(\nu_l)[(1 - N_{iu}) + \beta(1 - N_{iv})]$. Therefore,

$$G_{iu} = \frac{P^{\text{out}}_{iu}}{P^{\text{in}}_{iu}} = \exp\Big\{\Big[\big(\gamma_a(\nu_l) + \gamma_e(\nu_l)\big)(N_{iu} + \beta N_{iv}) - \gamma_a(\nu_l)(1+\beta)\Big] L_i\Big\} \tag{9}$$

(L_i is the length of the active fiber present in ring i). Concerning F_{iu}, it is convenient to express it as a function of the average powers, which are used as dynamic variables of the model (together with the relative populations N_{iu}). From Fig. 8 and (7) and (9), the following expression is straightforward:

$$P^s_{iiu} = \frac{2G_{iu}}{1+G_{iu}} T_{i,\text{out}} P_{iiu}, \tag{10}$$

whereas P^e_{iiu} is given by:

$$P^e_{iiu} = (1-w)P^s_{iiu} + w\big[\alpha P^s_{jiu} + (1-\alpha)P^s_{jiv}\big] \tag{11}$$

which can also be written as a function of the average powers:

$$P_{iiu}(i_{\text{in}}) = (1-w)\frac{2G_{iu}}{1+G_{iu}} T_{i,\text{out}} P_{iiu} + wT_{j,\text{out}} \times \left\{\alpha \frac{2G_{ju}}{1+G_{ju}} P_{jiu} + (1-\alpha)\frac{2G_{jv}}{1+G_{jv}} P_{jiv}\right\}. \tag{12}$$

From (11) and (12), F_{iu} can be expressed as:

$$F_{iu} = (1-w) + \frac{wT_{j,\text{out}}}{T_{i,\text{out}}} \frac{1+G_{iu}}{G_{iu}} \frac{\alpha \frac{G_{ju}P_{jiu}}{1+G_{ju}} + (1-\alpha)\frac{G_{jv}P_{jiv}}{1+G_{jv}}}{P_{iiu}}. \tag{13}$$

Finally, P_{iju} is obtained by means of:

$$P^{\text{in}}_{iju} = \big[\alpha P^{\text{out}}_{jju} + (1-\alpha)P^{\text{out}}_{jjv}\big] T_{i,\text{out}} w T_{j,\text{in}} \tag{14}$$

which, after straightforward algebra, leads to:

$$P_{iju} = \frac{1+G_{iu}}{2} P^{\text{in}}_{iju} = \frac{1+G_{iu}}{2} wT_{j,\text{out}} T_{i,\text{in}} \times \left\{\alpha \frac{G_{ju}}{1+G_{ju}} P_{jju} + (1-\alpha)\frac{G_{jv}}{1+G_{jv}} P_{jjv}\right\}. \tag{15}$$

A feedback term for P_{iju} similar to the one that accounts for P_{iiu} evolution (8) has not been included. If a term like this was considered, the model results were not good: only very fast transients without relaxation oscillations were obtained.

Note that P_{iju} can be expressed as a function of the P_{jju} and P_{jjv} variables. For calculations, the dynamic variables considered in the model are eight: N_{ax}, N_{ay}, N_{bx}, N_{by}, P_{aax}, P_{aay}, P_{bbx}, and P_{bby}. Their evolution equations are given by (2) and (8). The rest of the expressions provided relate the other variable magnitudes employed (G_{iu}, P_{iu}, P_{iju}) with the eight dynamic variables.

In the former expressions, we make use of several simplifications for the sake of the model plainness: the same

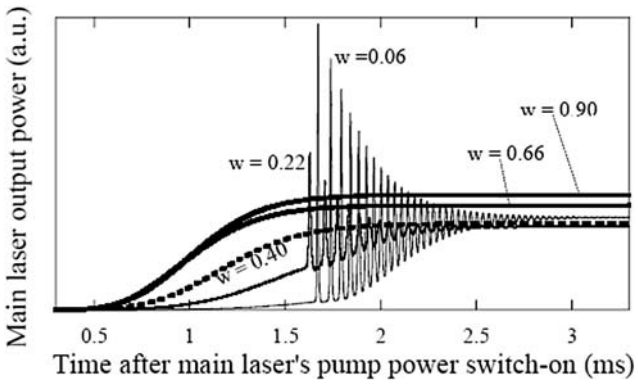

Fig. 9 Calculation of the temporal evolution of the main ring output laser emission after switch-on of its pump power, for several w values. Some parameter values employed are listed in Table 1. The rest are: $\delta_{ax} = 0.14$, $\delta_{bx} = 0.4$, $\beta_a = \beta_b = 0.75$, $\alpha = 0.15$, $P_{p,a} = 41$ mW, $P_{p,a} = 36$ mW

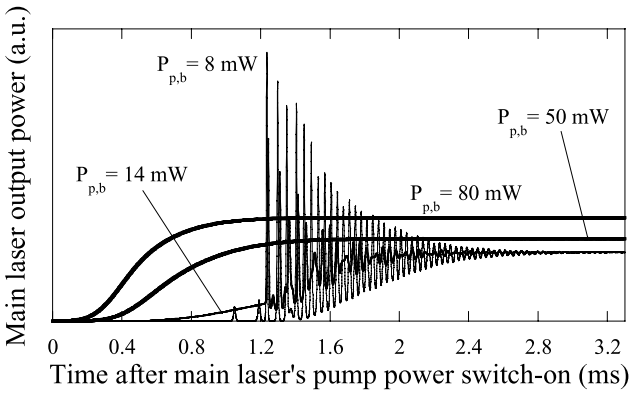

Fig. 10 Calculation of the temporal evolution of the main ring output laser emission after switch-on of its pump power, for several $P_{p,b}$ values. Some parameter values employed are listed in Table 1. The rest are: $\delta_{ax} = 0.20$, $\delta_{bx} = 0.3$, $\beta_a = 0.55$, $\beta_b = 0.854$, $\alpha = 0.7$, $P_{p,a} = 41$ mW, $w = 0.3$

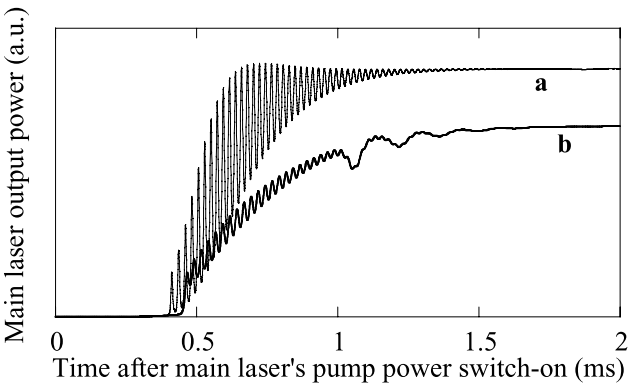

Fig. 11 Calculation of the temporal evolution of the main ring output laser emission after switch-on of its pump power. Some parameter values employed are listed in Table 1. The rest of the parameters common to curves (**a**) and (**b**) are: $P_{p,a} = 50$ mW, $P_{p,b} = 25$ mW and $\alpha = 0.7$. For curve (**a**): $\delta_{ax} = 0.3$, $\delta_{bx} = 0.4$, $\beta_a = 0.55$, $\beta_b = 0.80$, $w = 0.8$. For curve (**b**): $\delta_{ax} = 0.25$, $\delta_{bx} = 0.42$, $\beta_a = 0.55$, $\beta_b = 0.70$, $w = 0.6$

gain for mode u in ring i is considered both for λ_i and λ_j wavelengths, which seems reasonable provided that the wavelength mismatch is low (around 0.2 nm in good working conditions according to Fig. 5); also, the same passive transmission coefficients $T_{i,\text{in}}$ and $T_{i,\text{out}}$ are considered for λ_i and λ_j, although the losses introduced by the tuneable filter increase around 10% for a 0.2 nm mismatch between the wavelength introduced and the wavelength corresponding to the transmission maximum.

We show next the numerical results obtained with our model. Most of the parameters employed for the calculations are characteristic of our setup, while a few of them can be changed. The fixed parameters are listed in Table 1. The absorption and emission coefficients as well as the erbium concentration were determined following the procedure described in [26] and the methods for the determination of the rest of parameters in Table 1 are well-known. Changes experimentally observed when using the polarization controllers are considered in the model by allowing variations in the α, β and δ values (particularly, it was demonstrated in [27] that different β values could be obtained in a ring if different polarization states were selected by means of appropriate polarization controllers).

Figure 9 shows a series of transients numerically obtained, with all the parameters fixed save for the coupling between rings, w. Therefore, the model accounts for the different behaviors shown in Fig. 2. The same way, Fig. 10 shows another numerical series of transients for different $P_{p,b}$ powers, to be compared with the experimental series shown in Fig. 4. The qualitative agreement is also acceptable. Even some behaviors only rarely observed experimentally are also obtained theoretically (Fig. 11, to be compared with Fig. 7). It must be noted that most of the δ_{iu} values providing an acceptable agreement are closer to 0 or 1 than to 0.5. The physical interpretation of this fact is that an important proportion of the active ions is not efficiently pumped [28], which seems to be coherent with the high degree of polarization observed in the pump light launched to both rings (more than 95% in both cases).

In order to get a greater accuracy, the model could be complicated by considering spatial distributions of populations and laser powers instead of average quantities and even by considering longitudinal dependence of the interaction between polarization eigenmodes and assemblies. Nevertheless, it seems obvious that the resulting model would be very awkward and its usefulness very unclear: experimentally, it has been observed that simple changes in the bends and twists of the optical fiber induce changes in the light polarization state and in the laser output dynamics. Therefore, looking for accuracy in modelling a system whose output depends on working conditions so difficult to parameterize as the ones just mentioned does not seem worthwhile.

Table 1 Parameter values common to all calculations presented

Parameter	Value
Pump wavelength	1480 nm
Laser wavelength	1532 nm
Absorption coefficient at pump wavelength [$\gamma_a(\nu_p)$]	0.17 m^{-1}
Emission coefficient at pump wavelength [$\gamma_e(\nu_p)$]	0.06 m^{-1}
Absorption coefficient at laser wavelength [$\gamma_a(\nu_l)$]	1.22 m^{-1}
Emission coefficient at laser wavelength [$\gamma_e(\nu_l)$]	0.88 m^{-1}
Transmission factor $T_{a,\text{in}}$	0.40
Transmission factor $T_{a,\text{out}}$	0.20
Transmission factor $T_{b,\text{in}}$	0.80
Transmission factor $T_{b,\text{out}}$	0.23
Length of active fiber in ring a (L_a)	12 m
Length of active fiber in ring b (L_b)	26.9 m
Optical path of ring a (D_a)	55.8 m
Optical path of ring b (D_b)	88.0 m
Laser transition lifetime (τ)	10.5 ms
Er^{3+} ions per meter per assembly (N_t)	1.2×10^{13} m^{-1}

4 Conclusions

The transient behavior of an erbium-doped-fiber ring laser coupled to another one receiving CW pump power has been experimentally studied as a function of different system variables: degree of coupling between rings, pump powers launched to each ring, difference in wavelength tuning and polarization state selected by appropriate polarization controllers. Particularly, some results of interest for their potential applications have been found. On the one hand, smooth transient behaviors have been obtained. Besides, if the secondary laser is appropriately coupled to the main one, the latter reaches its steady state much faster than working on its own. On the other hand, instabilities in the laser output are obtained if both rings are tuned at very close wavelengths. This feature might be of interest as a basis for a tuning method with a precision of the order of one angstrom.

A model has been proposed which accounts for the different transient behaviors experimentally observed. For an acceptable performance of the model, inclusion of PHB is necessary. The agreement between the numerical and the experimental results is acceptable taking into account the system complexity, which makes unpractical a detailed treatment of some effects present in it. This agreement points out that all the mechanisms relevant to explain the dynamic behaviors experimentally obtained have been included in the model and, therefore, that the underlying physical phenomena taking place have been understood.

Acknowledgements This work was supported by the CICYT project FIS2006-03649.

References

1. C.L. Tang, H. Statz, G.A. DeMars, J. Appl. Phys. **34**, 2289 (1963)
2. K. Otsuka, P. Mandel, S. Bielawski, D. Derozier, P. Glorieux, Phys. Rev. A **46**, 1692 (1992)
3. S. Bielawski, D. Derozier, P. Glorieux, Phys. Rev. A **46**, 2811 (1992)
4. R. Leners, G. Stéphan, Quantum Semiclass. Opt. **7**, 757 (1995)
5. C.E. Preda, B. Ségard, P. Glorieux, Opt. Commun. **261**, 141 (2006)
6. O.G. Okhotnikov, J.R. Salcedo, Opt. Lett. **19**, 1445 (1994)
7. L.G. Luo, P.L. Chu, Opt. Commun. **149**, 307 (1998)
8. I.J. Sola, J.C. Martín, J.M. Álvarez, S. Jarabo, Opt. Commun. **193**, 133 (2001)
9. I.J. Sola, J.C. Martín, J.M. Álvarez, J. Mod. Opt. **53**, 525 (2006)
10. E. Lacot, F. Stoeckel, M. Chenevier, Phys. Rev. A **49**, 3997 (1994)
11. A.J. Poustie, Opt. Lett. **20**, 1868 (1995)
12. P. Mandel, M. Georgiou, K. Otsuka, D. Pieroux, Opt. Commun. **100**, 341 (1993)
13. K. Wiesenfeld, C. Bracikowski, G. James, R. Roy, Phys. Rev. Lett. **65**, 1749 (1990)
14. J. Wang, P. Mandel, Phys. Rev. A **48**, 671 (1993)
15. E. Siegmann, *Lasers* (University Science Books, Mill Valley, 1986)
16. Y.T. Chieng, G.J. Cowle, Electron. Lett. **30**, 1419 (1994)
17. V. Mizrahi, D.J. Digiovanni, R.M. Atkins, S.G. Grubb, Y.G. Park, J.M.P. Delavaux, J. Lightw. Tech. **12**, 2021 (1993)
18. P.A. Porta, L.M. Hoffer, H. Grassi, G.L. Lippi, Phys. Rev. A **61**, 33801 (2000)
19. G.L. Lippi, S. Barland, N. Dokhane, F. Monsieur, P.A. Porta, H. Grassi, L.M. Hoffer, J. Opt. B: Quantum Semiclass. Opt. **2**, 375 (2000)

20. B. Ségard, S. Matton, P. Glorieux, Phys. Rev. A **66**, 053819 (2002)
21. J.U. Kang, R. Sova, Electron. Lett. **36**, 1361 (2000)
22. I.J. Sola, J.C. Martín, J.M. Álvarez, Opt. Commun. **212**, 359 (2002)
23. S.S. Wang, H.G. Winful, Appl. Phys. Lett. **52**, 1774 (1988)
24. H.G. Winful, S.S. Wang, Appl. Phys. Lett. **53**, 1894 (1988)
25. www.aragonphotonics.com
26. I.J. Sola, J.C. Martín, J.M. Álvarez, Opt. Commun. **203**, 349 (2002)
27. J.C. Martín, Laser Phys. **15**, 1646 (2005)
28. J. Used, J.A. Sánchez-Martín, J.C. Martín, Fiber Integr. Opt. (2009, to be published)